M&C 2017 - International Conference on Mathematics & Computational Methods Applied to Nuclear Science & Engineering, Jeju, Korea, April 16-20, 2017, on USB (2017)

Implementation of Molten Salt Reactor Tools in SCALE[1]

Benjamin R. Betzler,* Jeffrey J. Powers,* Nicholas R. Brown,† and Bradley T. Rearden,*

*Oak Ridge National Laboratory, P.O. Box 2008, Oak Ridge, TN
†The Pennsylvania State University, 229 Reber Building, University Park, PA
betzlerbr@ornl.gov*

Abstract - *To support molten salt reactor commercialization, tools for calculating molten salt reactor fuel composition and reactivity changes during operation are being developed. Leveraging the capabilities of the SCALE code system, a one-dimensional delayed neutron precursor drift model has been implemented in the TRITON/NEWT transport module. With the fuel loop length, core height, fluid velocity, and core axial power shape, this model calculates the concentration of each delayed neutron precursor group within the one-dimensional loop. The model uses correction factors generated from these axially dependent concentrations to calculate the flow-adjusted parameters for the fission spectrum (χ^f) and the total number of neutrons per fission ($\bar{\nu}^f$) for the transport solver and cross section collapse. The SCALE implementation performs well in comparisons to analytic solutions of the one-dimensional model. This capability is demonstrated in an application to a TRITON/NEWT model of a unit cell of the Molten Salt Breeder Reactor. Results show nearly 40% of the total delayed neutrons are emitted outside of the core. A large fraction of the delayed neutrons drift to downstream low-power (in-core) regions, largely augmenting the delayed neutron source in these regions. The small axial region adjacent to the core outlet experiences a delayed neutron source that is over six times what is produced locally from fissions (as would be assumed for a no-drift transport calculation). For this application, differences between the no-drift solution and using the flow-adjusted parameters is up to 1%–2% in k_{eff} and some collapsed two-group constants.*

I. INTRODUCTION

Oak Ridge National Laboratory (ORNL) has recently undertaken work to advance the technology readiness level of a software package capable of calculating molten salt reactor (MSR) fuel composition and reactivity changes during operation. This work will prepare a prototype MSR neutronics tool that can be further applied to specific MSR designs, including those being developed by several private companies (e.g., Transatomic Power, Terrestrial Energy, FLiBe Energy). The recent $1.3B in private investment in advanced reactor technology detailed in a Third Way report [1] includes several of these leading liquid-fueled MSR concepts; this provides a growing need for an MSR neutronics and fuel cycle tool (along with additional MSR transient and heat transfer analysis tools). Increased interest in advanced reactors resulted in White House meetings on the topic and ORNL partnerships on two funding opportunities (up to $40M) [2].

Though products from universities or internally developed tools provide partial capabilities for liquid fueled MSR analysis, there is currently no established tool for neutronics and fuel cycle design and evaluation of liquid-fueled MSRs. Significant work in fast and thermal MSR analysis has yielded workable tools that aim to solve these issues [3, 4, 5, 6, 7, 8, 9]. Recent work at ORNL developing software with these capabilities has established proven methods and concepts. Initial development of these methods used external Perl scripts to enable the analysis of a liquid-fueled system with a solid-fueled reactor analysis tool [10]. This method grew into a generic Python script known as ChemTriton, which relied on the same methodology but provided more flexibility to analyze realistic scenarios in MSR operations [11, 12]. Separate efforts at ORNL are focused on developing tools for MSR whole core analysis with transport, depletion, and thermal hydraulics [13].

For neutronic and fuel cycle analysis, the two most important factors are depletion with continuous removals and delayed neutron precursor flow. Any tool attempting to properly model neutron transport and depletion in a fluid-fueled system must account for both of these phenomena. Implementation of these tools into SCALE [14] stands to benefit a larger number of analysis tools, as some tools use ORIGEN [15] for depletion calculations. This includes benefits to Shift [16] and other tools that use ORIGEN through its API. The discussion in this paper focuses on the implementation of a delayed neutron precursor drift model in SCALE.

[1]Notice: This manuscript has been authored by UT-Battelle, LLC, under Contract No. DE-AC0500OR22725 with the U.S. Department of Energy. The United States Government retains and the publisher, by accepting the article for publication, acknowledges that the United States Government retains a non-exclusive, paid-up, irrevocable, world-wide license to publish or reproduce the published form of this manuscript, or allow others to do so, for the United States Government purposes. The Department of Energy will provide public access to these results of federally sponsored research in accordance with the DOE Public Access Plan (http://energy.gov/downloads/doe-public-access-plan).

II. TRANSPORT WITH DELAYED NEUTRON PRECURSOR DRIFT

SCALE uses both deterministic (TRITON/NEWT [17]) and Monte Carlo (TRITON/KENO [18]) methods to provide flux or reaction rate information for depletion calculations. This information is passed to ORIGEN through coupling modules. Currently there is no delayed precursor drift model. While accounting for moving fuel in Monte Carlo and deterministic tools may be notably different, the implementation is based on the additional term in the neutron transport and precursor equations [19],

$$\frac{1}{v}\frac{\partial\psi}{\partial t} + \hat{\mathbf{\Omega}}\cdot\nabla\psi + \Sigma\psi(\mathbf{r}, E, \hat{\mathbf{\Omega}}, t) = \iint \Sigma_s(E', \hat{\mathbf{\Omega}}' \to E, \hat{\mathbf{\Omega}})\psi' dE' d\mathbf{\Omega}' + \sum_j^J \frac{\chi_j}{4\pi}\lambda_j C_j + \iint \frac{\chi_p}{4\pi}(1-\beta)\bar{\nu}\Sigma_f\psi' dE' d\mathbf{\Omega}' + \frac{S}{4\pi}, \text{ and} \quad (1)$$

$$\frac{\partial C_j}{\partial t} + \nabla\cdot\mathbf{u}C_j(\mathbf{r}, t) + \lambda_j C_j = \iint \beta_j\bar{\nu}\Sigma_f\psi' dE' d\mathbf{\Omega}', \quad \text{for} \quad j = 1, \ \ldots, \ J, \quad (2)$$

where

ψ is the angular flux,
C_j is the precursor concentration,
j denotes the precursor group,
$\mathbf{r}, E, \hat{\mathbf{\Omega}}, t$ describes the position-energy-direction-time phase space,
v is the neutron speed,
Σ is the total macroscopic cross section,
Σ_s is the scattering cross section from $E', \hat{\mathbf{\Omega}}'$ to $E, \hat{\mathbf{\Omega}}$,
χ_p is the prompt fission emission spectrum,
β is the total delayed neutron fraction,
$\bar{\nu}$ is the average neutrons released per fission,
Σ_f is the fission cross section,
χ_j is the delayed neutron emission spectrum,
λ_j is the delayed precursor decay constant,
S is the isotropic external source,
β_j is the group delayed neutron fraction, and
$\mathbf{u}$ is the vector describing the precursor flow.

The first term of Eq. 1 is the time-dependent variation of the flux, normally omitted in the steady-state formulation. The next six terms describe neutron interactions with material: leakage from the phase space, collisions, in-scatter, prompt fission, delayed fission, and external source. For simplicity, this formulation uses precursor density equations to describe delayed neutron emission. For each group j, Eq. 2 describes the time-dependent variation of the precursor density with three terms: precursor movement, precursor loss because of decay, and precursor source from fission.

Delayed neutron emission occurs as a result of typically less than 1% of fissions. When a heavy nucleus fissions, it splits into two or more fission products and neutrons. A small percentage of these fissions release a product known as a delayed neutron precursor. Delayed neutron precursors are radioactive, and upon decaying, release a neutron known as a delayed neutron. The release time of a delayed neutron depends on the half-life of the delayed neutron precursor. The energy of a delayed neutron is often much less than a prompt fission neutron and depends on the excited state of the delayed neutron precursor [20]. For ^{235}U, nuclear data sheets categorize the approximately 40 delayed neutron precursors into $J = 6$ groups according to their half-lives [21]. Each group has its own characteristic energy distribution, decay constant, and emission probability (Table I).

The delayed neutron emission spectrum and prompt fission emission spectrum are not equal. In addition, $\bar{\nu}$ is energy- and material-dependent and is defined as

$$\bar{\nu}(\mathbf{r}, E) = \bar{\nu}_p(\mathbf{r}, E) + \bar{\nu}_d(\mathbf{r}, E), \quad (3)$$

where $\bar{\nu}_p$ and $\bar{\nu}_d$ are the number of prompt and delayed neutrons emitted per fission event, respectively. In some formulations, this notation (Eq. 3) is preferred because (1) it uses a more basic quantity, $\bar{\nu}_d$, and (2) measurements show that $\bar{\nu}_d$ at typical energies in power reactors is independent of energy [20]. Thus, the energy variation in $\bar{\nu}$ is nearly entirely attributable to $\bar{\nu}_p$.

Many formulations (Eqs. 1 and 2) use β to define the energy-dependent fraction of delayed neutrons emitted,

$$\beta = \frac{\bar{\nu}_d}{\bar{\nu}}, \quad (4)$$

and unnormalized β_j to define the fraction of these delayed neutrons in each precursor group,

$$\beta_j = \alpha_j\beta, \quad (5)$$

where α_j is the energy-independent normalized group emission probability (Table I). These quantities are not to be confused with β_{eff}, which is an energy- and space-dependent quantity.

In a solid fuel reactor (e.g., a light water reactor), the fission product–delayed neutron precursors are located very near the fission site of their birth. The distance between the fission site and the precursor location is negligible; most transport codes effectively ignore this distance to simplify calculations. For a liquid fuel reactor, these precursors move with the flowing fuel material before decaying and releasing a delayed neutron. In some cases, the precursor may flow outside of the core and decay within the fuel loop. This effectively reduces the number of delayed neutrons emitted in the core. Longer-lived precursors may flow through the fuel loop and reenter the core before decaying. The effect on k_{eff} of this precursor drift

TABLE I. Six Group Delayed Neutron Data for ^{235}U

j	λ_j [s^{-1}]	normalized β_j (α_j)
1	0.0125	0.0320
2	0.0318	0.1664
3	0.109	0.1613
4	0.317	0.4596
5	1.35	0.1335
6	8.64	0.0472

is on the order of a few hundred pcm and must be appropriately characterized to properly calculate the delayed neutron source.

Characteristics of the fuel flow depend on the fuel loop dimensions, core dimensions and geometry, and mass flow rates. The main interest of this effort is to obtain the steady-state distribution of precursors in the core as a function of position; this is necessary to properly quantify the effect that the precursor drift has on the SCALE neutronic solution. TRITON/NEWT is limited to two-dimensional geometries, while TRITON/KENO is capable of simulating three-dimensional noninfinite geometries.

1. Transport Solutions

The TRITON/NEWT transport tool (as well as many other transport tools) are designed for steady state analysis, focusing on the solution of the transport equation [17],

$$\hat{\mathbf{\Omega}} \cdot \nabla\psi + \Sigma(\mathbf{r}, E)\psi(\mathbf{r}, E, \hat{\mathbf{\Omega}}) = Q(\mathbf{r}, E, \hat{\mathbf{\Omega}}), \tag{6}$$

where Q is the source at $\mathbf{r}, E, \hat{\mathbf{\Omega}}$, and

$$Q(\mathbf{r}, E, \hat{\mathbf{\Omega}}) = S(\mathbf{r}, E, \hat{\mathbf{\Omega}}) + F(\mathbf{r}, E, \hat{\mathbf{\Omega}}) + S_{\text{ext}}(\mathbf{r}, E). \tag{7}$$

The three terms in Q are the scattering source (S), fission source (F), and external/fixed source (S_{ext}), where

$$S(\mathbf{r}, E, \hat{\mathbf{\Omega}}) = \iint \Sigma_s(\mathbf{r}; E', \hat{\mathbf{\Omega}}' \rightarrow E, \hat{\mathbf{\Omega}})\psi' dE' d\mathbf{\Omega}', \text{ and} \tag{8}$$

$$F(\mathbf{r}, E, \hat{\mathbf{\Omega}}) = \iint \frac{\chi(\mathbf{r}, E)}{4\pi} \bar{\nu}(\mathbf{r}, E')\Sigma_f(\mathbf{r}, E')\psi' dE' d\mathbf{\Omega}', \tag{9}$$

and χ is the normalized combined fission-delayed neutron emission spectrum.

This steady-state formulation (Eqs. 6–9) does not explicitly use delayed neutron parameters; instead it accounts for delayed neutron precursors in the lumped quantities $\bar{\nu}$ (Eq. 3) and χ,

$$\chi = \chi_p(1 - \beta) + \sum_{j=1}^{J} \chi_j \beta_j. \tag{10}$$

Accounting for the delayed neutron precursor drift with TRITON/NEWT and similar tools requires the definition and use of the flow-adjusted parameters $\bar{\nu}^{\text{f}}$ and χ^{f},

$$\bar{\nu}^{\text{f}} = \bar{\nu}_p + \bar{\nu}_d^{\text{f}}, \text{ and} \tag{11}$$

$$\chi^{\text{f}} = \chi_p(1 - \beta^{\text{f}}) + \sum_{j=1}^{J} \chi_j \beta_j^{\text{f}}, \tag{12}$$

where $\beta_j^{\text{f}}, \beta^{\text{f}}$, and $\bar{\nu}_d^{\text{f}}$ are flow-adjusted parameters,

$$\bar{\nu}_d^{\text{f}}(\mathbf{r}, E) = \bar{\nu}_d(\mathbf{r}, E)\frac{\beta^{\text{f}}}{\beta}, \text{ and} \tag{13}$$

$$\beta^{\text{f}} = \frac{\bar{\nu}_d^{\text{f}}}{\bar{\nu}}. \tag{14}$$

This formulation is entirely dependent on the calculated flow-adjusted group delayed neutron fractions (β_j^{f}), which must reflect the loss of neutrons outside of the core. The fraction on the right side of Eq. 13 is dependent only on flow characteristics and may be calculated before the transport calculation. The combined fission-delayed neutron emission spectrum (Eq. 12) is dependent on the problem-specific spectrum and must be estimated.

2. Zero-Dimensional Drift

Zero-dimensional delayed neutron precursor drift methods simplify the problem into two conditions for delayed neutron emission: (1) inside and (2) outside of the core. A simplified approximation is obtained by considering the fuel loop characteristics: mass flow rate ($\dot{m}$), the mass fraction of the fuel salt in the active core (f_{core}), and the mass of fuel in the fuel loop (m_{loop}). These factors define the flow-adjusted delayed neutron fraction of each delayed precursor group, which may be approximated with

$$\beta_j^{\text{f}} \approx \frac{\beta_j}{\int e^{-\lambda_j t} dt} \left(\int_0^{\frac{\Delta t_{\text{core}}}{2}} e^{-\lambda_j t} dt + \sum_{i=1}^{\infty} \int_{(i-\frac{1}{2})\Delta t_{\text{core}} + i\Delta t_{\text{loop}}}^{(i+\frac{1}{2})\Delta t_{\text{core}} + i\Delta t_{\text{loop}}} e^{-\lambda_j t} dt \right), \tag{15}$$

$$\Delta t_{\text{core}} = \frac{f_{\text{core}} m_{\text{loop}}}{\dot{m}}, \text{ and} \tag{16}$$

$$\Delta t_{\text{loop}} = \frac{(1 - f_{\text{core}}) m_{\text{loop}}}{\dot{m}}, \tag{17}$$

where λ_j is the group j delayed neutron precursor decay constant, Δt_{core} is the average time it takes for a molecule to pass through the active core, and Δt_{loop} is the average time it takes for a molecule to pass through the fuel loop outside the core.

This approximation simply obtains the fraction of decays of precursor group j that occur within the active core. It is based on the flow of the average molecule in the fuel salt and assumes a typical cosine axial power shape (i.e., the average neutron is born at the axial core midplane). It is possible to include fewer terms in the summation, as the successive terms decrease exponentially. Integration (Eq. 15) yields a simpler equation for the flow-adjusted delayed neutron fractions,

$$\beta_j^{\text{f}} \approx \beta_j \left[\left(1 - e^{-\frac{\lambda_j \Delta t_{\text{core}}}{2}} \right) + \left(e^{\frac{\lambda_j \Delta t_{\text{core}}}{2}} - e^{-\frac{\lambda_j \Delta t_{\text{core}}}{2}} \right) \sum_{i=1}^{\infty} e^{-\lambda_j i(\Delta t_{\text{core}} + \Delta t_{\text{loop}})} \right]. \tag{18}$$

This is the zero-dimensional simplified model.

More complex models are dependent on some simplified form of the neutron transport or point kinetics equations. Consider the exact point kinetics equations describing the amplitude $p(t)$ and neutron precursor concentrations $c_j(t)$,

$$\frac{dp(t)}{dt} = \frac{\rho(t) - \bar{\beta}(t)}{\Lambda(t)} p(t) + \sum_j \lambda_j c_j(t) + s(t), \text{ and} \tag{19}$$

$$\frac{dc_j(t)}{dt} = -\lambda_j c_j(t) + \frac{\bar{\beta}_j(t)}{\Lambda(t)} p(t), \quad \text{for } j = 1, \ldots, J, \tag{20}$$

with the definitions

$$\rho(t) = \frac{1}{F(t)} \int_V \int_0^\infty \phi_0^\dagger(\mathbf{r}, E)(-\mathbf{M} + \mathbf{F})\psi(\mathbf{r}, E, t) dE dV, \quad (21)$$

$$c_j(t) = \frac{1}{F(t)\Lambda(t)} \int_V \int_0^\infty \phi_0^\dagger(\mathbf{r}, E)\chi_j(E) C_j(\mathbf{r}, t) dE dV, \quad (22)$$

$$\bar{\beta}_j(t) = \frac{1}{F(t)} \int_V \int_0^\infty \phi_0^\dagger(\mathbf{r}, E)\chi_j \mathbf{F}_{\mathbf{d}\,j}\psi(\mathbf{r}, E, t) dE dV, \quad (23)$$

$$\bar{\beta}(t) = \sum_j \beta_j(t), \quad (24)$$

$$\Lambda(t) = \frac{K_0}{F(t)}, \quad (25)$$

$$s(t) = \frac{1}{F(t)\Lambda(t)} \int_V \int_0^\infty \phi_0^\dagger(\mathbf{r}, E) S(\mathbf{r}, E, t) dE dV, \text{ and} \quad (26)$$

$$F(t) = \int_V \int_0^\infty \phi_0^\dagger(\mathbf{r}, E)\mathbf{F}\psi(\mathbf{r}, E, t) dE dV, \quad (27)$$

for the kinetic parameters: reactivity $\rho(t)$, group j effective delayed neutron fractions $\bar{\beta}_j$, and prompt neutron lifetime $\Lambda(t)$. This factorization approach does not introduce an approximation [20].

With or without delayed neutron precursor drift, after long operation times (i.e., $t \to \infty$) the precursor concentrations approach equilibrium concentrations. Without delayed neutron precursor drift, the equilibrium concentrations are described mathematically (Eq. 20) as

$$\lambda_j c_j = \frac{\bar{\beta}_j}{\Lambda} p. \quad (28)$$

With delayed neutron precursor drift, the precursor concentration equation (Eq. 20) becomes

$$\frac{dc_j(t)}{dt} = -\lambda_j c_j(t) + \frac{\bar{\beta}_j(t)}{\Lambda(t)} p(t) - \frac{c_j(t)}{\tau_c} + \frac{c_j(t - \tau_e)e^{-\lambda_j \tau_e}}{\tau_c}, \quad (29)$$

where τ_c is transit time through the core and τ_e is the transit time through the external loop [22, 23]. These two additional terms describe the rate of precursors leaving the core and the rate of reentry by precursors that left the core τ_L seconds ago and have decayed to a fraction of their previous value [22]. Applying the same time conditions (i.e., $t \to \infty$) that yielded Eq. 28 and reworking the equation yields

$$\lambda_j c_j = \frac{\bar{\beta}_j}{\Lambda} p \left(\frac{\tau_c \lambda_j}{\tau_c \lambda_j + 1 - e^{-\lambda_j \tau_e}} \right). \quad (30)$$

This is equivalent to Eq. 28 with an additional factor that defines the fraction of delayed neutron precursors that decay within the core. Using this factor to recalculate the flow-adjusted delayed neutron fractions yields the zero-dimensional model:

$$\beta_j^{\mathrm{f}} \approx \beta_j \left(\frac{\tau_c \lambda_j}{\tau_c \lambda_j + 1 - e^{-\lambda_j \tau_e}} \right). \quad (31)$$

3. One-Dimensional Drift

One-dimensional delayed neutron precursor drift methods normally simplify the problem into an axially dependent partial differential equation similar to Eq. 20,

$$\frac{\partial c_j(z,t)}{\partial t} + v(z,t)\frac{\partial c_j(z,t)}{\partial z} = -\lambda_j c_j(z,t) + \frac{\bar{\beta}_j(t)}{\Lambda(t)} p(z,t), \quad (32)$$

where v is the space- and time-dependent velocity of the fluid. Applying the same time conditions that yielded Eqs. 28 and 30 (i.e., $t \to \infty$) yields the simpler ordinary differential equation (ODE),

$$v(z)\frac{dc_j(z)}{dz} = -\lambda_j c_j(z) + \frac{\bar{\beta}_j}{\Lambda} p(z). \quad (33)$$

Without drift, this ODE is similar to Eq. 28,

$$\lambda_j c_j(z) = \frac{\bar{\beta}_j}{\Lambda} p(z). \quad (34)$$

With drift, the analytical solution to Eq. 33 is obtained with and integrating factor,

$$\lambda_j c_j(z) = \lambda_j e^{-V(z)} \int e^{V(z)} Q(z) dz + A\lambda_j e^{-V(z)}, \quad (35)$$

where A is a constant and $V(z)$ and $Q(z)$ are

$$V(z) = \int \frac{\lambda_j}{v(z)} dz, \text{ and} \quad (36)$$

$$Q(z) = \frac{\bar{\beta}_j p(z)}{\Lambda v(z)}. \quad (37)$$

This is analytically solvable for simple problems, and is numerically solvable for more complex systems. In any case, it is useful to define the entire fuel loop (i.e., $0 < z < L$) with the equations to define the appropriate boundary conditions (Fig. 1),

$$c_{j,\mathrm{core}}^-(H) = c_{j,\mathrm{loop}}^+(H), \text{ and} \quad (38)$$

$$c_{j,\mathrm{loop}}^-(L) = c_{j,\mathrm{core}}^+(0), \quad (39)$$

where H is the length of the core and $c_{j,\mathrm{core}}$ and $c_{j,\mathrm{loop}}$ represent the precursor concentrations in the core and in the loop.

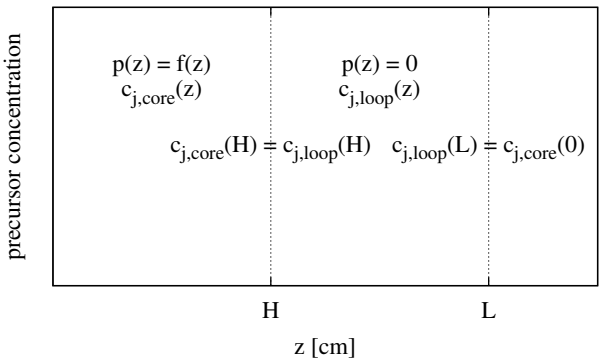

Fig. 1. The one-dimensional precursor drift problem showing boundary conditions.

Together these two functions describe a piecewise continuous function that arises from the piecewise power function $p(z)$,

$$p(z) = f(z) \text{ for } 0 < z < H, \text{ and} \tag{40}$$

$$p(z) = 0 \text{ for } H < z < L, \tag{41}$$

where $f(z)$ is some arbitrary function, and it is assumed that there is no power generated in the loop (effectively true in most cases). In the loop, the description of the precursor concentrations (Eq. 35) simplifies to

$$\lambda_j c_{j,\text{loop}}(z) = B\lambda_j e^{-V(z)}, \tag{42}$$

where B is a constant.

These solutions for precursor drift are incorporated into the neutron transport solution considering (1) the precursor concentrations at a specific location in the core or (2) the average precursor concentrations over a given axial range. In both considerations, the objective is to compare the solution of the one-dimensional drift, $c_{j,\text{drift}}$, to the solution without drift, $c_{j,\text{v=0}}$, to obtain the correction factor, F_j, for group j,

$$\beta_j^{\text{f}} \approx \beta_j F_j. \tag{43}$$

This axially dependent correction factor is

$$F_j(z) = \frac{c_{j,\text{drift}}(z)}{c_{j,\text{v=0}}(z)}. \tag{44}$$

Integrating the top and bottom of Eq. 44 yields the range-average correction factor,

$$F_j = \frac{\int_{z_1}^{z_2} c_{j,\text{drift}}(z)dz}{\int_{z_1}^{z_2} c_{j,\text{v=0}}(z)dz}, \tag{45}$$

which is the one-dimensional model. If $z_1 = 0$ and $z_2 = H$, the resulting F_js are core-averaged. The factor used to adjust $\bar{\nu}_d$ on the right side of Eq. 13 is simply the sum of the product of these group factors and the normalized group emission probabilities,

$$F(z) = \sum_{j=1}^{J} F_j(z)\alpha_j, \text{ and} \tag{46}$$

$$F = \sum_{j=1}^{J} F_j \alpha_j. \tag{47}$$

For the calculation of the correction factors, the difference between the problem-dependent quantities $\bar{\beta}$ (Eq. 23) and Λ (Eq. 25) is ignored. These parameters are slightly different when calculated from the transport solution with and without the precursor drift model.

The current application focus for these SCALE tools is on thermal MSRs, which incorporate some moderating structure material to the core and contains channels through which salt flows. These types of problems are ideal candidates for a simplified one-dimensional precursor drift model, which ignores the profile of the fluid velocity within the flow channel or structure and quickly delivers solutions for the precursor concentration within the fuel loop. For these problems, it is assumed that a one-dimensional model is sufficient to approximate the effect of precursor drift. This model is likely insufficient for the more complex fuel flows in fast spectrum MSR cores, which are primarily made up of free flowing salt fuel and incorporate little structure into the design.

III. IMPLEMENTATION AND TESTING

Implementation of the precursor drift model in TRITON/NEWT requires two major developments: (1) a mechanism for correcting the delayed neutron fractions and energy spectra, and (2) an ODE solver to obtain the precursor concentrations as a function of dimension (Eq. 33). Several changes are necessary to achieve the former. Currently, TRITON/NEWT reads in the total average number of neutrons emitted per fission ($\bar{\nu}$, MT = 452) from ENDF-6–formatted data and generates a combined (prompt and delayed) fission emission spectrum ($\bar{\chi}$, MT = 1,018) from ENDF-6–formatted data. Before the full transport calculation, these quantities are calculated for each mixture (i.e., unique material composition) in the problem, where

$$\bar{\nu}_g = \frac{\sum_i^M N_i \sigma_{fig} \bar{\nu}_{ig}}{\sum_i^M N_i \sigma_{fig}}, \text{ and} \tag{48}$$

$$\bar{\chi}_g = \sum_i^M \left(\bar{\chi}_{ig} N_i \sum_{g'}^G \bar{\nu}_{ig'} \sigma_{fig'} \phi_{ig'} \right), \tag{49}$$

where

$\bar{\nu}_g$ is the total average number of neutrons emitted per fission for the mixture in group g,

M is the total number of nuclides,

N_i is the atom density of nuclide i,

σ_{fig} is the microscopic fission cross section for nuclide i and group g,

$\bar{\nu}_{ig}$ is the average number of neutrons emitted per fission for nuclide i and group g,

$\bar{\chi}_g$ is the combined fission emission probability for the mixture in group g,

$\bar{\chi}_{ig}$ is the combined fission emission probability for nuclide i in group g, and

ϕ_{ig} is the normalized flux integral for nuclide i in group g from the calculation.

For use in transport calculations, Eq. 49 is normalized, and the mixture $\bar{\nu}_g$ is folded into the quantity $\Sigma_{fg}\bar{\nu}_g$. The combined quantities in Eqs. 48 and 49 may be split into their prompt and delayed components,

$$\bar{\nu}_g = \frac{\sum_i^M N_i \sigma_{fig} \bar{\nu}_{pig}}{\sum_i^M N_i \sigma_{fig}} + \frac{\sum_i^M N_i \sigma_{fig} \bar{\nu}_{dig}}{\sum_i^M N_i \sigma_{fig}}, \text{ and} \tag{50}$$

$$\bar{\chi}_g = \sum_i^M \left(\chi_{pig} N_i \sum_{g'}^G \bar{\nu}_{pig'} \sigma_{fig'} \phi_{ig'} \right) + \sum_j^J \left[\sum_i^M \left(\chi_{djig} N_i \sum_{g'}^G \alpha_j \bar{\nu}_{dig'} \sigma_{fig'} \phi_{ig'} \right) \right], \tag{51}$$

where

$\bar{\nu}_{pig}$ and $\bar{\nu}_{dig}$ denote the prompt and delayed contributions to the total $\bar{\nu}_{ig}$,

χ_{pig} denotes the prompt emission spectra for nuclide i and group g, and χ_{djig} denotes the group j delayed emission spectra for nuclide i and group g.

To obtain the flow-adjusted parameters $\bar{\nu}_g^{\text{f}}$ and χ_g^{f}, the delayed contribution terms in Eqs. 50 and 51 are multiplied

by the adjustment factors (Eq. 46 or 47 and Eq. 44 or 45),

$$\bar{\nu}_g^{\mathrm{f}} = \frac{\sum_i^M N_i \sigma_{fig} \bar{\nu}_{pig}}{\sum_i^M N_i \sigma_{fig}} + F \frac{\sum_i^M N_i \sigma_{fig} \bar{\nu}_{dig}}{\sum_i^M N_i \sigma_{fig}}, \text{ and} \tag{52}$$

$$\bar{\chi}_g^{\mathrm{f}} = \sum_i^M \left(\chi_{pig} N_i \sum_{g'}^G \bar{\nu}_{pig'} \sigma_{fig'} \phi_{ig'} \right) + \sum_j^J \left[\sum_i^M \left(\chi_{djig} N_i \sum_{g'}^G F_j \alpha_j \bar{\nu}_{dig'} \sigma_{fig'} \phi_{ig'} \right) \right]. \tag{53}$$

To calculate these flow-adjusted parameters, the prompt (MT = 456) and delayed (MT = 455) contribution to $\bar{\nu}$ must be read from the cross section files. To calculate the adjustment factors (F_j), the delayed neutron (MT = 455) group decay constants (λ_j) and relative emission fractions (α_j) must also be read from the cross section files. Currently, SCALE libraries do not contain some of this delayed neutron information. Decay constants and relative emission fractions (λ_j and α_j) of a few fissile isotopes are currently hard-coded in SCALE: ^{232}Th, ^{233}U, ^{235}U, ^{238}U, ^{239}Pu, ^{240}Pu, and ^{241}Pu. Some isotopes have a set of λ_j and α_j for thermal and fast fission. While the SCALE libraries contain a χ_p spectra (MT = 1,056), this is not currently shared with the working library available to TRITON/NEWT. The χ_d spectra (MT = 1,055) in the SCALE libraries is an averaged spectrum from all the delayed groups combined (χ_{dig}); there is no information on the group-specific χ_{dj}. Without this group-specific information, the calculation of the flow-adjusted spectrum (Eq. 53) simplifies to

$$\bar{\chi}_g^{\mathrm{f}} = \sum_i^M \left(\chi_{pig} N_i \sum_{g'}^G \bar{\nu}_{pig'} \sigma_{fig'} \phi_{ig'} \right) + F \sum_i^M \left(\chi_{dig} N_i \sum_{g'}^G \bar{\nu}_{dig'} \sigma_{fig'} \phi_{ig'} \right). \tag{54}$$

A backward Euler method is implemented to solve the ODE (Eq. 33) for each precursor group. This ODE is solved with the backward Euler method iteratively (with different initial conditions) until the boundary conditions are satisfied (Eqs. 38 and 39). A numerical integration method is used to perform the necessary integrals to determine the range-integrated ratios (Eq. 45).

For the simplest one-dimensional problem (Eqs. 35 and 42), the velocity and power are constants, resulting in the following analytical solutions:

$$\lambda_j c_{j,\mathrm{core}} = \lambda_j \left(\frac{Q}{V} + A e^{-V_z} \right), \tag{55}$$

$$\lambda_j c_{j,\mathrm{loop}} = B \lambda_j e^{-V_z}, \tag{56}$$

$$Vz = \frac{\lambda_j}{v} z, \tag{57}$$

$$Q = \frac{\bar{\beta}_j p}{\Lambda v}, \tag{58}$$

$$A = \frac{Q}{V} \left(\frac{e^{VH} - e^{VL}}{e^{VL} - 1} \right), \text{ and} \tag{59}$$

$$B = \frac{Q}{V} \left(\frac{e^{VH} - 1}{1 - e^{-VL}} \right). \tag{60}$$

The correction factors using these solutions are

$$F_j(z) = 1 + e^{-V_z} \left(\frac{e^{VH} - e^{VL}}{e^{VL} - 1} \right), \text{ and} \tag{61}$$

$$F_j = 1 + \frac{\left(e^{VH} - e^{VL} \right) \left(1 - e^{-VH} \right)}{VH \left(e^{VL} - 1 \right)}, \tag{62}$$

where F_j is averaged over the core. A more complex one-dimensional problem (Eqs. 35 and 42) uses constant velocity and a sinusoidal power shape,

$$p(z) = \frac{\pi}{2H} \sin \frac{\pi z}{H}. \tag{63}$$

The analytic solution without precursor drift (Eq. 34) is

$$\lambda_j c_j(z) = U \sin \frac{\pi z}{H}, \text{ and} \tag{64}$$

$$U = \frac{\bar{\beta}_j \pi}{2 \Lambda H}. \tag{65}$$

The analytic solution with precursor drift (Eqs. 35 and 42) is

$$\lambda_j c_{j,\mathrm{core}} = VUG \left(V \frac{H}{\pi} \sin \frac{\pi}{H} z - \cos \frac{\pi}{H} z \right) + A \lambda_j e^{-V_z}, \tag{66}$$

$$\lambda_j c_{j,\mathrm{loop}} = B \lambda_j e^{-V_z}, \tag{67}$$

$$A = \frac{VUG}{\lambda_j} \left(\frac{e^{VL} + e^{VH}}{e^{VL} - 1} \right), \tag{68}$$

$$B = \frac{VUG}{\lambda_j} \left(e^{VH} + \frac{e^{VL} + e^{VH}}{e^{VL} - 1} \right), \text{ and} \tag{69}$$

$$G = \frac{\frac{\pi}{H}}{V^2 + \left(\frac{\pi}{H} \right)^2}. \tag{70}$$

The correction factors using these solutions are

$$F_j(z) = \frac{VG}{\sin \frac{\pi}{H} z} \left[V \frac{H}{\pi} \sin \frac{\pi}{H} z - \cos \frac{\pi}{H} z + e^{-V_z} \left(\frac{e^{VL} + e^{VH}}{e^{VL} - 1} \right) \right], \text{ and} \tag{71}$$

$$F_j = \frac{VG\pi}{2H} \left[2V \left(\frac{H}{\pi} \right)^2 + \frac{\left(e^{VL} + e^{VH} \right) \left(1 - e^{-VH} \right)}{V \left(e^{VL} - 1 \right)} \right], \tag{72}$$

where F_j is averaged over the core.

Comparing these analytical solutions with numerical solutions from SCALE modules provides confidence in the solutions to more complex power and velocity profiles. The delayed neutron data (Table I) and flow loop information (Table II) is held constant for these test problems. Comparisons of the analytic zero-dimensional and core-averaged one-dimensional models highlights trends and deficiencies in some of the models (Table III). The zero-dimensional simplified model is more accurate for groups with smaller decay constants and performs poorly for the faster decaying precursor groups. The zero-dimensional model performs more consistently across the precursor groups, but it is unable to capture the effect on precursor concentration from axial power profiles. For the one-dimensional model, the factors are averaged over

the height of the core; the zero-dimensional models are unable to generate factors over smaller portions of the core (e.g., the bottom half of the core). As a result of these shortcomings, only the one-dimensional model is implemented in SCALE.

The axial distribution of precursors in the core-loop system is highly dependent on the decay constant and the power shape (Fig. 2). As the fuel flows, precursors generated in high power regions drift toward lower power regions and into the coolant loop. Precursors in groups with larger decay constants decay quickly; the axial distribution of these precursors is very similar to the no-drift solution. Precursors in groups with the smallest decay constants have relatively constant axial distributions. The region over the last several centimeters of the core ($310 < z < 340$ cm) has relatively low power, but it has a high precursor concentration as recently born precursors drift into the region. Conversely, the region over the first several centimeters of the core ($0 < z < 30$ cm) has a relatively low power and a low precursor concentration because many precursors decay within the loop before reentering the core.

With a constant or sinusoidal power profile, the analytical solutions and those generated by SCALE match for both axially dependent (Fig. 3) and core-averaged (Table IV) quantities. A constant power profile produces lower group correction factors for the first several centimeters, particularly for the fast-decaying precursor groups because precursors are unable to return to the core before decaying in the loop. The larger the decay constant of the precursor group, the lower the correction factors at the core inlet ($z = 0$ cm). At core outlet ($z = 340$ cm), the precursors in groups with the largest decay constants have the highest correction factors, as slowly decaying precursors enter the loop before decaying in the core. With a constant power profile, the correction factor is never greater than 1.0. A sinusoidal power profile produces more complex axial dependence in the correction factors. As the power approaches zero at the edges of the core, the correction factors increase above 1.0 as more precursors drift into these regions than are generated by the local fission rate. For the faster decaying precursor groups, precursors are unable to pass through the loop before decaying, and the correction factor at the core inlet is zero. For slower decaying precursor groups, some precursors make it to core inlet, and the correction factors become very large. The core outlet experiences a large increase in precursor concentration.

TABLE II. Flow Information for the Test Problems

Parameter	Value
H	340.0 cm
L	629.6 cm
v	47.72 cm/s

TABLE III. Analytic Correction Factors (F) Using Different Models

j	0-D Simp.	0-D	Core-averaged 1-D $p(z) = C$	Core-averaged 1-D $p(z) \sim \sin(z)$
1	0.5404	0.5493	0.5403	0.5403
2	0.5426	0.5635	0.5417	0.5421
3	0.6011	0.6480	0.5788	0.5885
4	0.8170	0.7772	0.7236	0.7660
5	0.9919	0.9059	0.8961	0.9518
6	1.0000	0.9840	0.9838	0.9987
total	0.7597	0.7405	0.6994	0.7287

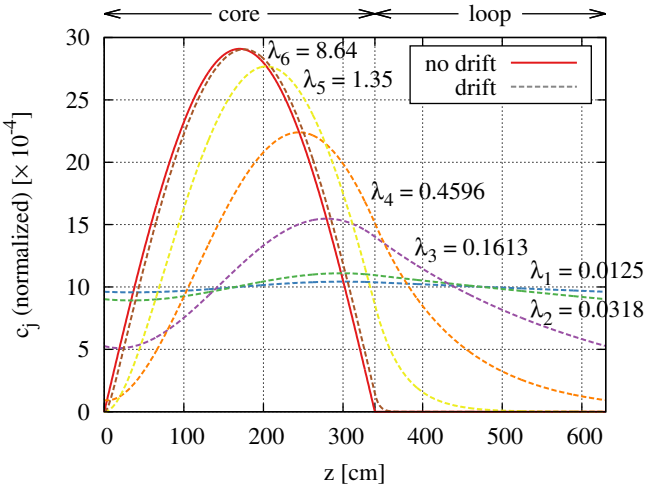

Fig. 2. Normalized solutions of the precursor concentration in the one-dimensional system for the six precursor groups with a sinusoidal power shape. Decay constants are in units of s^{-1}.

IV. APPLICATION TO A UNIT CELL PROBLEM

The implementation of the one-dimensional precursor drift model in TRITON/NEWT is tested for a simple unit cell problem (Fig. 4) based on the Molten Salt Breeder Reactor (Table V). Uranium and thorium tetrafluoride are dissolved in the FLiBe carrier salt, where the uranium is isotopically pure ^{233}U. The fuel salt composition is for a fresh (i.e., unirradiated) condition. Delayed neutron data is available for two isotopes in this problem: ^{233}U and ^{232}Th. This problem is solved using core-averaged correction factors and factors averaged over the last 15 cm of the core. A sinusoidal power distribution is assumed.

The calculated core-averaged correction factors are 0.6732 and 0.6322 for ^{232}Th and ^{233}U, respectively. Application of these correction factors slightly reduces the delayed component in the χ_t spectrum and decreases the $\bar{\nu}_t$ slightly (Fig. 5) with respect to the solutions without precursor drift.

TABLE IV. One-Dimensional Core-Averaged Correction Factors (F) with Different Power Profiles

j	Flat Power SCALE	Flat Power Analytic[(a)]	Sinusoidal Power SCALE	Sinusoidal Power Analytic[(a)]
1	0.5402	0.5403 (0.01)	0.5398	0.5403 (0.10)
2	0.5416	0.5417 (0.02)	0.5415	0.5421 (0.11)
3	0.5783	0.5788 (0.08)	0.5877	0.5885 (0.14)
4	0.7229	0.7236 (0.10)	0.7650	0.7660 (0.14)
5	0.8955	0.8961 (0.07)	0.9505	0.9518 (0.14)
6	0.9832	0.9838 (0.06)	0.9971	0.9987 (0.16)
tot.	0.6989	0.6994 (0.07)	0.7277	0.7287 (0.14)

[(a)] Relative difference (%) in parenthesis.

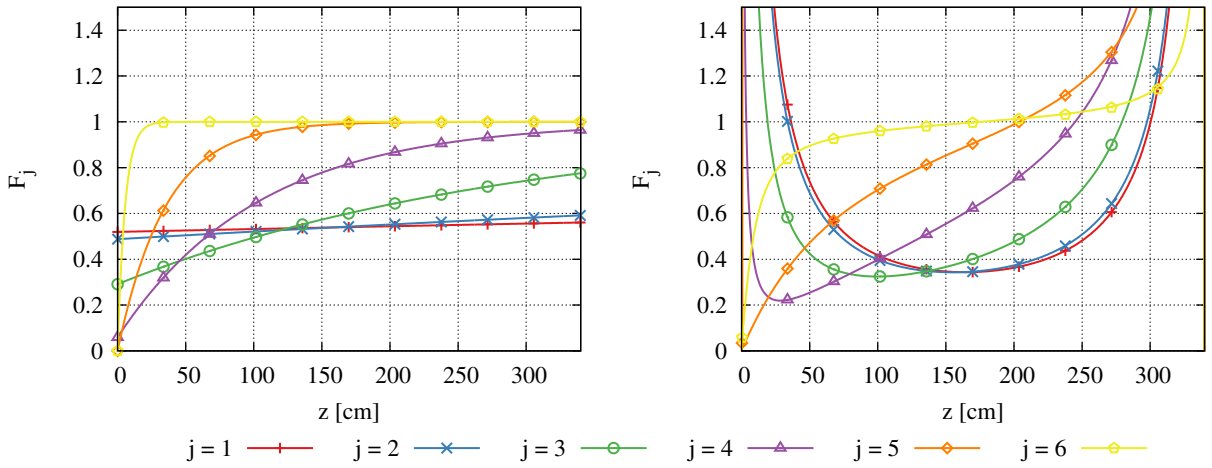

Fig. 3. Comparison of the axially dependent group correction factors, $F_j(z)$, from SCALE and analytical solutions with constant (left) and sinusoidal (right) power profiles. Analytical solutions are plotted as a line, and solutions from SCALE are plotted as points.

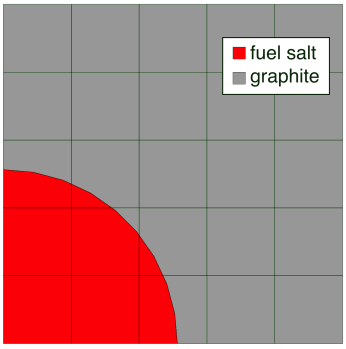

Fig. 4. TRITON/NEWT unit cell.

These differences are very small and are most noticeable for the lowest probabilities in the χ_t spectrum. The $\bar{\nu}_t$ changes less than 0.7% for all energy groups.

Averaging the last 15 cm of the core produces much larger correction factors because of the precursors drifting into the region before entering the coolant loop: 6.5467 and 6.3874 for ^{232}Th and ^{233}U, respectively. Application of these correction factors increases the delayed neutron component in the χ_t spectrum and $\bar{\nu}_t$ (Fig. 6) with respect to the solutions without precursor drift. While the change in the spectrum is more significant than the change for the core-averaged case, it is only noticeable for the lowest probabilities of the χ_t spectrum. There is an increase of up to 11% in the $\bar{\nu}_t$, peaking around 2–4 MeV.

Despite the large difference in the delayed contribution to χ_t when accounting for precursor drift, use of the flow-adjusted spectrum has little impact on criticality calculations (Table VI). This delayed contribution is too small to have a significant effect on k. Conversely, the use of the flow-adjusted $\bar{\nu}_t$ has a very large effect on criticality calculations and accounts for most of the change in k when using both flow-adjusted parameters. The large increase in delayed neutron precursors

TABLE V. Unit Cell Problem Characteristics

Parameters	Value	
fuel temperature [K]	909	
graphite temperature [K]	900	
graphite density [g/cc]	1.843	
fuel channel radius [cm]	2.59917	
fuel channel pitch [cm]	10.16	
cross section library	252-group ENDF/B-VII.1 [24]	
fuel isotopic composition [g/cc]	^{19}F	1.48999
	^{233}U	0.02397
	^{232}Th	1.43197
	^{7}Li	0.25870
	^{9}Be	0.07416

TABLE VI. TRITON/NEWT-Calculated k Using Different Flow-Corrected Constants

Condition	Core-averaged		Last 15 cm	
	NEWT k	Δk [pcm]	NEWT k	Δk [pcm]
no drift	1.06984	—	1.06984	—
with $\bar{\nu}_t^{\mathrm{f}}$	1.06867	−117	1.08738	1,754
with $\bar{\chi}_t^{\mathrm{f}}$	1.06984	0	1.06997	13
with $\bar{\nu}_t^{\mathrm{f}}$, $\bar{\chi}_t^{\mathrm{f}}$	1.06867	−117	1.08749	1,765
est. $\Delta k^{(a)}$	—	*−116*	—	*1,710*

[(a)] From Eq. 73

in the last 15 cm toward the outlet of the core cause a change in k of over 1,500 pcm with the flow-adjusted $\bar{\nu}_t$. For this thermal system, fission in ^{233}U dominates, and the effect on the calculated k using the correction factors is estimated by

$$\Delta k = k_{\text{no drift}} \left(F_{\text{U-233}} - 1\right) \beta_{\text{U-233}}, \tag{73}$$

where $\beta_{\text{U-233}}$ is approximately 296 pcm [24]. The TRITON/NEWT-calculated k eigenvalues agree fairly well with these estimated values.

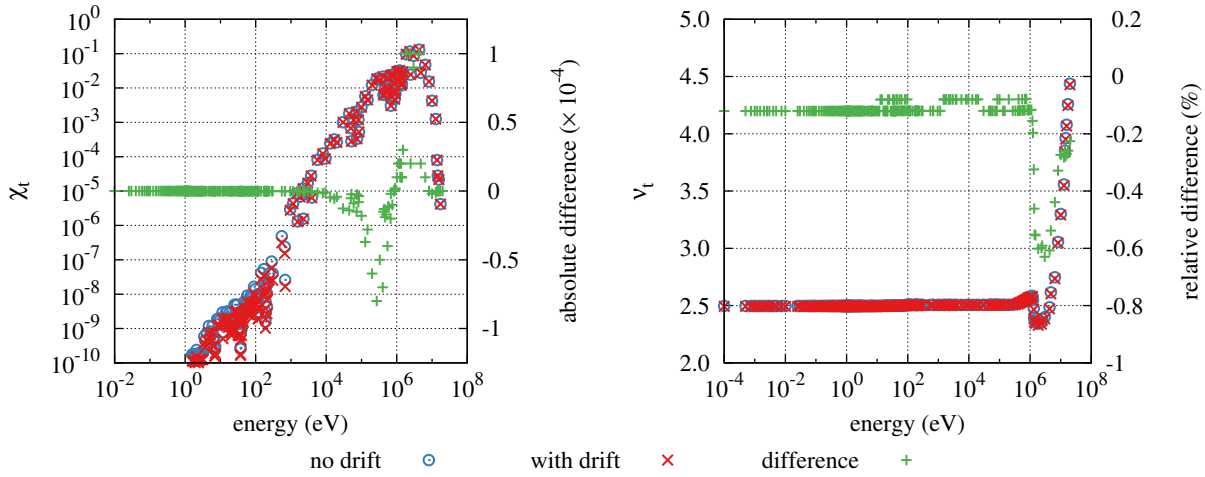

Fig. 5. The flow-adjusted χ_t (left) and $\bar{\nu}_t$ (right) using the core-averaged correction factors.

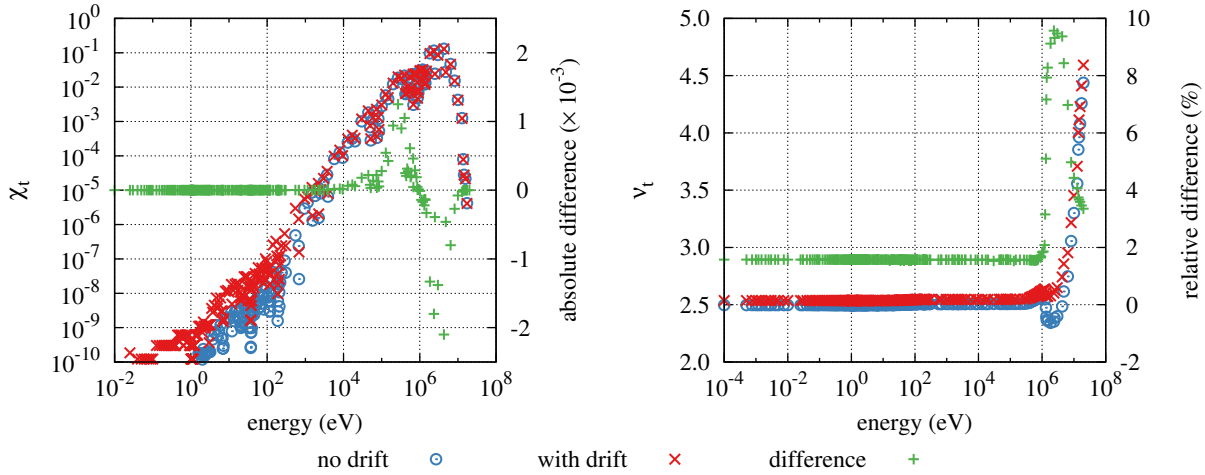

Fig. 6. The flow-adjusted χ_t (left) and $\bar{\nu}_t$ (right) using the correction factors averaged over the last 15 cm of the core.

Despite the large differences in calculated k when using the drifted parameters, the TRITON/NEWT-calculated multi-group flux solution is only slightly affected by use of the flow-adjusted parameters (Fig. 7). The largest differences are observed in the fast energy ranges. This is reflected in the two-group collapsed cross sections, where the change in this spectrum mainly affects the fast group constants in addition to $\bar{\nu}\Sigma_f$ (Table VII).

V. CONCLUSIONS AND FUTURE WORK

A one-dimensional delayed neutron precursor drift method has been implemented in TRITON/NEWT. The implementation has been tested using some comparisons to zero-dimensional models and analytical solutions with simplified power and velocity profiles. Applications to a unit cell model of the Molten Salt Breeder Reactor examine the χ and $\bar{\nu}$ parameters, calculated k_{eff}, calculated spectrum, and collapsed two-group constants with and without the precursor drift model. The TRITON/NEWT-calculated flow-adjusted k_{eff} agrees well with simple theoretical expectations. The effect on the calculated quantities is examined for different elevations in the MSR loop. The two-group cross sections perform fairly well for this thermal system (i.e., in comparisons between the k_{eff} and k_∞), suggesting that a more complex group structure may not be needed for nodal diffusion calculations.

Lessons learned from this implementation inform future work. There is a minimal effect from the use of a flow-adjusted χ spectrum to account for the augmented number of delayed neutrons at a given location in the loop. This is because the delayed neutron contribution to χ is only slightly more thermal than the prompt neutron contribution and makes up a small amount of the total contribution. The majority of the effect on the calculation is captured with a flow-adjusted $\bar{\nu}$; correcting for the number of delayed neutrons emitted at a given location in the loop should be the main focus of future efforts.

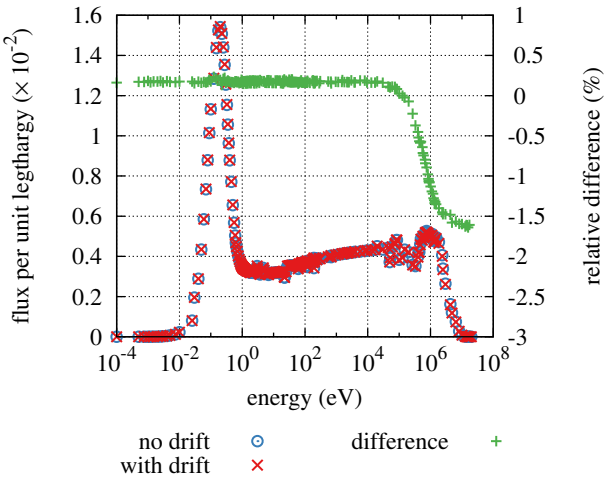

Fig. 7. Normalized neutron flux in the two-dimensional unit cell with and without precursor drift (using flow-adjusted constants from correction factors averaged over the last 15 cm of the loop).

TABLE VII. TRITON/NEWT-Calculated Two-Group Cross Sections Using Different Flow-Corrected Constants

Constant	No drift	Middle 15 cm[a]	Last 15 cm[a]
$k_{\text{eff}}^{(b)}$	1.06984	1.06820 (0.15)	1.08749 (1.62)
$k_{\infty}^{(c)}$	1.07034	1.06868 (0.16)	1.08796 (1.62)
$\Sigma_{\text{tr},1}$	0.32781	0.32776 (0.02)	0.32839 (0.18)
$\Sigma_{\text{tr},2}$	0.40862	0.40862 (0.00)	0.40862 (0.00)
$\Sigma_{\text{a},1} \times 10^{-3}$	1.66403	1.66370 (0.02)	1.66771 (0.22)
$\Sigma_{\text{a},2} \times 10^{-3}$	5.63859	5.63859 (0.00)	5.63859 (0.00)
$(\bar{\nu}\Sigma_{\text{f}})_1 \times 10^{-3}$	1.24340	1.24108 (0.19)	1.26791 (1.93)
$(\bar{\nu}\Sigma_{\text{f}})_2 \times 10^{-3}$	7.13632	7.12545 (0.15)	7.25026 (1.57)
$\Sigma_{1,2} \times 10^{-3}$	3.73485	3.73403 (0.02)	3.74442 (0.26)

[a] Absolute difference (%) in parenthesis.
[b] From NEWT transport.
[c] Using two-group cross sections.

Ongoing work includes the implementation of continuous removals in SCALE and building a user interface to interact with these tools. This also includes the potential implementation of the drift model into a SCALE Monte Carlo capability. This may be performed using direct sampling of a delayed fission and precursor decay event or other approximate methods to avoid the larger computational burden from the additional sampling. These capabilities are currently planned for release in SCALE 6.3.

VI. ACKNOWLEDGMENTS

This work is supported by the US Department on Energy, Office of Technology Transitions, Technology Commercialization Fund. The authors would like to thank Matthew A. Jessee for his help with implementation in TRITON/NEWT.

REFERENCES

1. S. BRINTON, "The Advanced Nuclear Industry," http://www.thirdway.org/report/the-advanced-nuclear-industry, Third Way (June 2015), Accessed March 1, 2016.
2. "FACT SHEET: Obama Administration Announces Actions to Ensure that Nuclear Energy Remains a Vibrant Component of the United States' Clean Energy Strategy," https://www.whitehouse.gov/the-press-office/2015/11/06/fact-sheet-obama-administration-announces-actions-ensure-nuclear-energy, White House, Office of the Press Secretary (November 2015), Accessed August 8, 2016.
3. H. F. BAUMAN, G. W. CUNNINGHAM III, ET AL., "ROD: A Nuclear and Fuel-Cycle Analysis Code for Circulating-Fuel Reactors," Tech. Rep. ORNL-TM-3359, Oak Ridge National Laboratory (1971).
4. D. HEUER, E. MERLE-LUCOTTE, ET AL., "Towards the Thorium Fuel Cycle with Molten Salt Reactors," *Annals of Nuclear Energy*, **64**, 421–429 (2014).
5. C. FIORINA, M. AUFIERO, ET AL., "Investigation of the MSFR core physics and fuel cycle characteristics," *Progress in Nuclear Energy*, **68**, 153–168 (2013).
6. R. J. SHEU, C. H. CHANG, ET AL., "Depletion Analysis on Long-Term Operation of the Conceptual Molten Salt Actinide Recycler & Transmuter (MOSART) by Using a Special Sequence Based on SCALE6/TRITON," *Annals of Nuclear Energy*, **53**, 1–8 (2013).
7. M. AUFIERO, A. CAMMI, ET AL., "An Extended Version of the SERPENT-2 Code to Investigate Fuel Burn-Up and Core Material Evolution of the Molten Salt Fast Reactor," *Journal of Nuclear Materials*, **441**, 473–486 (2013).
8. A. AHMAD, E. B. MCCLAMROCK, and A. GLASER, "Neutronics Calculations for Denatured Molten Salt Reactors: Assessing Resource Requirements and Proliferation-Risk Attributes," *Annals of Nuclear Energy*, **75**, 261–267 (2015).
9. J. PARK, Y. JEONG, ET AL., "Whole Core Analysis of Molten Salt Breeder Reactor with Online Fuel Reprocessing," *International Journal of Energy Research*, **39**, 1673–1680 (2015).
10. J. J. POWERS, T. J. HARRISON, and J. C. GEHIN, "A New Approach for Modeling and Analysis of Molten Salt Reactors Using SCALE," in "Proc. Int. Conf. Mathematics and Computational Methods Applied to Nuclear Science and Engineering (M&C 2013)," Sun Valley, Idaho (2013).
11. B. R. BETZLER, J. J. POWERS, and A. WORRALL, "Modeling and Simulation of the Start-up of a Thorium-Based Molten Salt Reactor," in "Proc. Int. Conf. PHYSOR 2016," Sun Valley, Idaho (2016).
12. B. R. BETZLER, J. J. POWERS, and A. WORRALL, "Molten Salt Reactor Neutronics and Fuel Cycle Modeling and Simulation with SCALE," *Annals of Nuclear Energy*, **101**, 489–503 (2017).
13. B. COLLINS, C. GENTRY, and S. STIMPSON, "Molten Salt Reactor Capability Using MPACT," in "Proc. Int. Conf. on Mathematics and Computational Methods Ap-

plied to Nuclear Science and Engineering (M&C 2017)," Jeju, Korea (2017).

14. B. T. REARDEN and M. A. JESSEE, "SCALE Code System," ORNL/TM-2005/39, Version 6.2, Oak Ridge National Laboratory, Oak Ridge, Tennessee (June 2016). Available from Radiation Safety Information Computational Center at Oak Ridge National Laboratory as CCC-834.
15. I. C. GAULD, G. RADULESCU, ET AL., "Isotopic Depletion and Decay Methods and Analysis Capabilities in SCALE," *Nuclear Technology*, **174**, 267–283 (2011).
16. G. G. DAVIDSON, T. M. PANDYA, ET AL., "Nuclide Depletion Capabilities in the Shift Monte Carlo Code," in "Proc. Int. Conf. PHYSOR 2016," Sun Valley, Idaho (2016).
17. M. D. DEHART and S. M. BOWMAN, "Reactor Physics Methods and Analysis Capabilities in SCALE," *Nuclear Technology*, **174**, *2*, 196–213 (2011).
18. S. GOLUOGLU, L. M. PETRIE JR., ET AL., "Monte Carlo Criticality Methods and Analysis Capabilities in SCALE," *Nuclear Technology*, **174**, 214–235 (2011).
19. C. NICOLINO, G. LAPENTA, ET AL., "Coupled Dynamics in the Physics of Molten Salt Reactors," *Annals of Nuclear Energy*, **35**, 314–322 (2008).
20. K. O. OTT and D. A. MENELY, *Introductory Nuclear Reactor Dynamics*, American Nuclear Society, La Grange Park, Illinois (1985).
21. M. B. CHADWICK, P. OBLOZINKY, ET AL., "ENDF/B-VII.0: Next Generation Evaluated Nuclear Data Library for Nuclear Science and Technology," *Nuclear Data Sheets*, **107**, 2931–3060 (2006).
22. S. J. BALL and T. W. KERLIN, "Stability Analysis of the Molten-Salt Reactor Experiment," Tech. Rep. ORNL-TM-1070, Oak Ridge National Laboratory (1965).
23. A. CAMMI, C. FIORINA, ET AL., "Dimensional Effects in the Modelling of MSR Dynamics: Moving on from Simplified Schemes of Analysis to a Multi-physics Modelling Approach," *Nuclear Engineering and Design*, **246**, 12–26 (2012).
24. M. B. CHADWICK, P. OBLOZINKY, ET AL., "ENDF/B-VII.1: Nuclear Data For Science and Technology: Cross Sections, Covariance, Fission Product Yields and Decay Data," *Nuclear Data Sheets*, **112**, 2887–2996 (2011).